ISSN 0036-0295, Russian Metallurgy (Metally), Vol. 2020, No. 5, pp. 540–548. © Pleiades Publishing, Ltd., 2020.
Russian Text © The Author(s), 2020, published in Metally, 2020, No. 3, pp. 41–50.

Solidification and the Structure-Phase State of Ni_3Al–Ni–NiAl Alloys with Chromium, Molybdenum, Tungsten, Rhenium, and Cobalt

K. B. Povarova[a, *], A. A. Drozdov[a, b], O. A. Bazyleva[c], M. A. Bulakhtina[a], A. E. Morozov[a], A. V. Antonova[a], E. G. Arginbaeva[c], and Yu. V. Loshchinin[c]

[a] *Baikov Institute of Metallurgy and Materials Science, Russian Academy of Sciences, Moscow, Russia*
[b] *Bardin TsNIIChermet, Moscow, Russia*
[c] *All-Russia Research Institute of Aviation Materials, Moscow, Russia*
**e-mail: povarova@imet.ac.ru*

Received November 13, 2019; revised November 29, 2019; accepted December 3, 2019

Abstract—The ternary Ni–Al–AE phase diagrams, where AEs are the main alloying elements of high-temperature cast (γ′ + γ) γ′-Ni_3Al-based alloys, are analyzed. Principal differences between the solidification schemes in the vicinity of the γ′-Ni_3Al and β-NiAl phases and the differences in the characters of the influence of the main AEs at their contents to 10 at % on the phase composition and the structure of multicomponent γ′-Ni_3Al-based VKNA-1V, VKNA-25, VKNA-4U, and IM730 alloys are detcted. The structural base of all the alloys are (γ′ + γ) dendrites. In the first-type cobalt-free VKNA1V alloys, as well as in IC221M, IC218, IC438, and IC6SX alloys, coarse single-phase γ′-Ni_3Al precipitates, which are the degenerate eutectic $L \rightleftarrows (\gamma' + \gamma) + \gamma'$, form in the interdendritic space. In the second-type cobalt-containing alloys at the same (~17 at %) aluminum content (VKNA-4U, VKNA-25) or in the chromium-containing cobalt-free alloys with an increased (~21 at %) aluminum content (IM730), the following two-phase precipitates form: the nonequilibrium β-NiAl phase, which represents the degenerate $L \rightleftarrows (\gamma' + \beta) + \beta$ eutectic, forms inside γ′-Ni_3Al. The following solid-phase transformations are found to develop intensely in the second-type alloys on heating in the temperature range 1200–1300°C: the dissolution of the β-phase precipitates in the primary γ′-Ni_3Al precipitates, the dissolution or a weakening of the interdendritic γ′-phase precipitates, and a change in the morphology and orientations of the γ-phase precipitates in dendrites and the interdendritic space.

Keywords: phase diagrams, reaction schemes, nickel aluminide, cast alloys, phase transformations, structures

DOI: 10.1134/S0036029520050109

INTRODUCTION, FORMULATION OF THE PROBLEM

In the recent two decades, the cast alloys based on the intermetallic γ′-Ni_3Al compound are considered as promising light high-temperature materials capable of operating at temperatures to 1100–1200°C for a long time and up to 1250–1300°C for a short time. These alloys are intended and used for manufacturing operating and nozzle blades, nozzle folds, combustion chambers, and other important parts of gas-turbine engines (GTEs) of civil and military aviation [1–4]. They are high-melting and light and have a high-temperature strength as compared to modern nickel superalloys (SA). The high characteristics of cast heterophase (γ′-Ni_3Al + γ-Ni) alloys of the VKNA type with a single-crystal structure are determined, first, by the fact the their heterophase structure with coherent or semicoherent bonding between the γ′ and γ phases with ordered ($L1_2$) and disordered fcc crystal structures, respectively, is conserved to the solidus temperature, unlike the SAs in which the single-phase γ region $[(\gamma + \gamma') \rightarrow \gamma \rightarrow (\gamma + L)]$ exists in the temperature range $T_{solv} \le T \le T_{solid}$, which leads to a softening of nickel SAs due to the dissolution of the strengthening γ′-Ni_3Al phase. The existence of 10–15 vol % γ-Ni (nickel-based solid solution which is a viscous structural component) in the alloys provides a high low-temperature plasticity of the alloys and, as a result, the possibility of refusing from microalloying with boron, which is an obligatory component of the alloys, such as IC221M, IC218 [5], IC438 and others, developed in Oak Ridge National Laboratory (United States) and also the IC6SX alloy developed in Lockheed Martin Energy Res. (United States). In these alloys, boron determines the plasticity due to its joint segregation with nickel on grain boundaries and the formation of layers with disordered structure there.

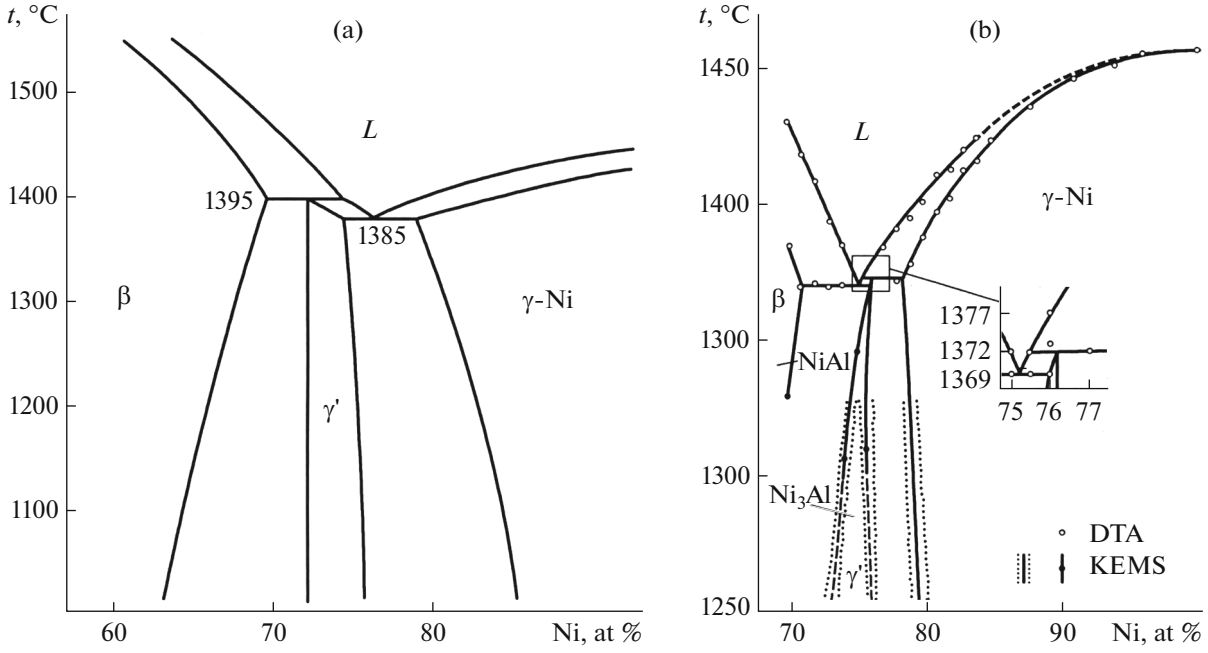

Fig. 1. (a) First and (b) second variants of the binary Ni–Al phase diagram (KEMS are the data of the Knudsen effusion mass-spectroscopy).

Intermetallic multicomponent alloys have a complex structure–phase state, which is dependent on the proportion of components, melting and solidification conditions, and heat treatment (HT). The distribution of alloying elements (AEs) in single crystals and in ingots of the multicomponent intermetallic alloys formed by equiaxial solidification is determined by the scheme of phase transformations during the solidification, which can be changed within a relatively narrow concentration range so that the γ'-Ni_3Al, β-NiAl, or γ-Ni can be a leading phase. The study of the possibility to increase the high-temperature strength characteristics of these alloys and to optimize their structure–phase states revealed certain contradictions of interpreting the role of dendrite microsegregation, the existence of coarse primary γ'-Ni_3Al precipitates in the interdendritic space, and even the composition and the structure of these precipitates in the alloys of this type.

The base systems for developing high-temperature nickel superalloys and the alloys based on nickel aluminide γ'-Ni_3Al are binary Ni–Al phase diagrams (PDs), ternary PDs, and, what is rarely, the portions of multicomponent PDs.

There are two main variants of binary Ni–Al PDs [6, 7] (Fig. 1), which differ in an alloy solidification scheme. In the first variant (Fig. 1a), the γ'-Ni_3Al phase precipitates according to the peritectic reaction L + β-$Ni_3Al \rightleftarrows$ γ'-Ni_3Al and forms a eutectic with γ-Ni, $L \rightleftarrows$ γ' + γ. In the second variant (Fig. 1b), the γ'-Ni_3Al phase precipitates during the peritectic reaction L + γ-Ni $\rightleftarrows$ γ'-Ni_3Al and forms a eutectic with β-NiAl, $L \rightleftarrows$ γ'-Ni_3Al + β-NiAl. The temperatures of these reactions differ insignificantly (3–10°C).

In the ternary and multicomponent PDs of the Ni–Al–X–Y type, the situation becomes still less determined, since four-phase equilibrium and the transition of one solidification scheme to another are possible in them even at insignificant change in the composition of a multicomponent alloy. In this connection, the interpretations of the structure-phase states of cast (γ' + γ) alloys can be different, the more so that the morphology of the structural components, which is commonly our "guide" as we solve points open to questions, is dependent in many respects on the solidification temperature and conditions.

It should be noted, in particular, the existence of so-called additional phases in the nickel aluminide-based multicomponent alloys, which exist only in nickel superalloys. They can be not only interstitial phases (complex oxides, carbides, nitrides, and borides), but also topologically close-packed (TCP) phases, such as σ, ε, χ, and τ formed by high-melting AEs, among them are AEs containing nickel [8–11]. The formation of coarse inclusions of some of them can be prevented using the melting method proposed in our works (stage-by-stage introduction of elements taking into account their reaction capabilities); however, nanoparticles of these phases significantly influence the high-temperature strength of the alloys [12, 13].

Table 1. Chemical compositions, at %, of nickel-based intermetallic multicomponent alloys

Alloy	Al	Ti, Zr, Hf	Co	Cr	Re	REM, B	W	Mo
VKNA-1V	17.2	1.8 Ti, 0.14 Hf	–	6.0	–	0.015 La	1.0	1.8
VKNA-25	17.5	0.6 Ti	4.2	6.2	0.42	0.01 La	0.9	2.9
VKNA-4U	17.2	1.1 Ti	3.7	5.2	–	–	0.6	2.3
IM730	20.9	0.11 Zr	–	7.0	–	0.1 B	–	0.91

All our works were based on the point of view that the multicomponent alloys are solidified by the first of the abovementioned schemes. However, the analysis of the microstructures of a number of alloys in the states after solidification [14, 15] and the study of the specific features of the dendrite segregation [16–18] showed that other solidification schemes are also possible. Because the mechanical properties of cast alloys (strength, high-temperature strength, creep resistance, plasticity under conditions of static, variable, and sign-changing loads, and so on) are dependent on the structure-phase state of the alloys formed during their solidification and subsequent HT, it is necessary to study the solidification schemes in the vicinity of nickel aluminides γ′-Ni_3Al and β-NiAl and to establish the correlation between the solidification schemes, the structure, and the high-temperature strength of the cast alloys.

The aim of this work is to analyze our experimental data on the structure of two groups of γ′-Ni_3Al-based alloys with different types of alloying and solidification schemes.

EXPERIMENTAL

We studied Ni–Al–Cr–Mo–Ti(Zr, Hf)–La(B) alloys with W, Re, and Co or without them, which were based on nickel aluminides γ′-Ni_3Al and β-NiAl. Table 1 gives the alloy compositions and the summary contents of heavy high-melting AEs in them. The alloys were manufactured on the production bases of VIAM (VKNA type) and TsNIIchermet (IM730).

The alloys were melted using the following charge materials: N1 nickel, A99 aluminum, ERX-1 electrolytic chromium, MSh-V metallic molybdenum in the shape of a bar, zirconium iodide, and Ni–10 wt % B and NiLa master alloys. The VKNA-type alloys with a directional structure were produced from charge billets smelted in a vacuum induction furnace with a basic lining with subsequent high-gradient directional solidification (HGDS) at a gradient $g = 150°C/cm$ and rate $R = 5$, 10, and 20 mm/min from a seed with crystallographic orientation (CGO) [111] or [001]. The structure of the rods 16 mm in diameter and 170–180 mm in length met the following conditions (without macroboundaries): the deviation of the given CGO direction was ≤10°, the misorientation between blocks was ≤6°. The IM730 alloy with a polycrystalline structure was melted in an induction furnace (Al_2O_3 lining) in air (open heat) under slag. All the alloys were melted in induction furnaces using the method of sequent introduction of components into a melt taking into account their reaction activities: Ni (Ni + slag for the IM730 alloy), NiW master alloy, Mo, Co, Cr, and Ti + Al + Hf/Zr + NiLa master alloy in several portions. During the equiaxial solidification of the IM730 alloy, the melted metal was fed in a mold made of electrode corundum and armasil aqueous binder.

The alloy microstructures were studied by optical microscopy (OM) and scanning electron microscopy (SEM; Olympus GX51, Carl Zeiss LEO-1420, JEOL JSM-840, FEI Scios microscopes). SEM micrographs were taken in the secondary-electron (SE) and backscattered (BSE) modes. EDX analysis was carried out on the same electron microscopes using Oxford and EDAX energy-dispersive microanalyzers. Differential thermal analysis (DTA) was performed by differential scanning calorimetry (DSC) on a DSC 404 F1 differential scanning calorimeter on heating and cooling at a rate of 20 K/min in a helium atmosphere.

RESULTS AND DISCUSSION

Structures of the High-Temperature (γ′ + γ) Alloys

Figures 2 and 3 show the characteristic structures of the (γ′ + γ) Ni–Al–Cr–Mo(W)–Ti(Zr)–(Co)–(Re)–La(B) alloys in the state after solidification. The alloys have a single-crystal (SC) and polycrystalline (PC) structures. The structure of the VKNA-4U alloy (with cobalt, but rhenium-free) is similar to the VKNA-25 (with cobalt and rhenium) alloy.

As seen from Figs. 2 and 3, all the alloys have a dendrite–cellular structure independent of the solidification method: HGDS or upon centrifugal pouring Figs. 2a, 2c, 2e).

We focus attention on the difference between the dendrite structures of cobalt-free and rhenium-free VKNA-1V alloys and the VKNA-25 alloy containing these AEs. The dendrites of both alloys have a two-phase structure: the γ′-phase portions several micrometers in size are separated by interlayers of nickel-based γ-solid solution with thickness not more than 0.2–0.5 μm. In the VKNA-1V alloy, the γ-phase interlayers are discontinuous; the γ′-phase portions have irregular shapes; the structure resembles an eutectic one formed during solidification (Fig. 2b). The struc-

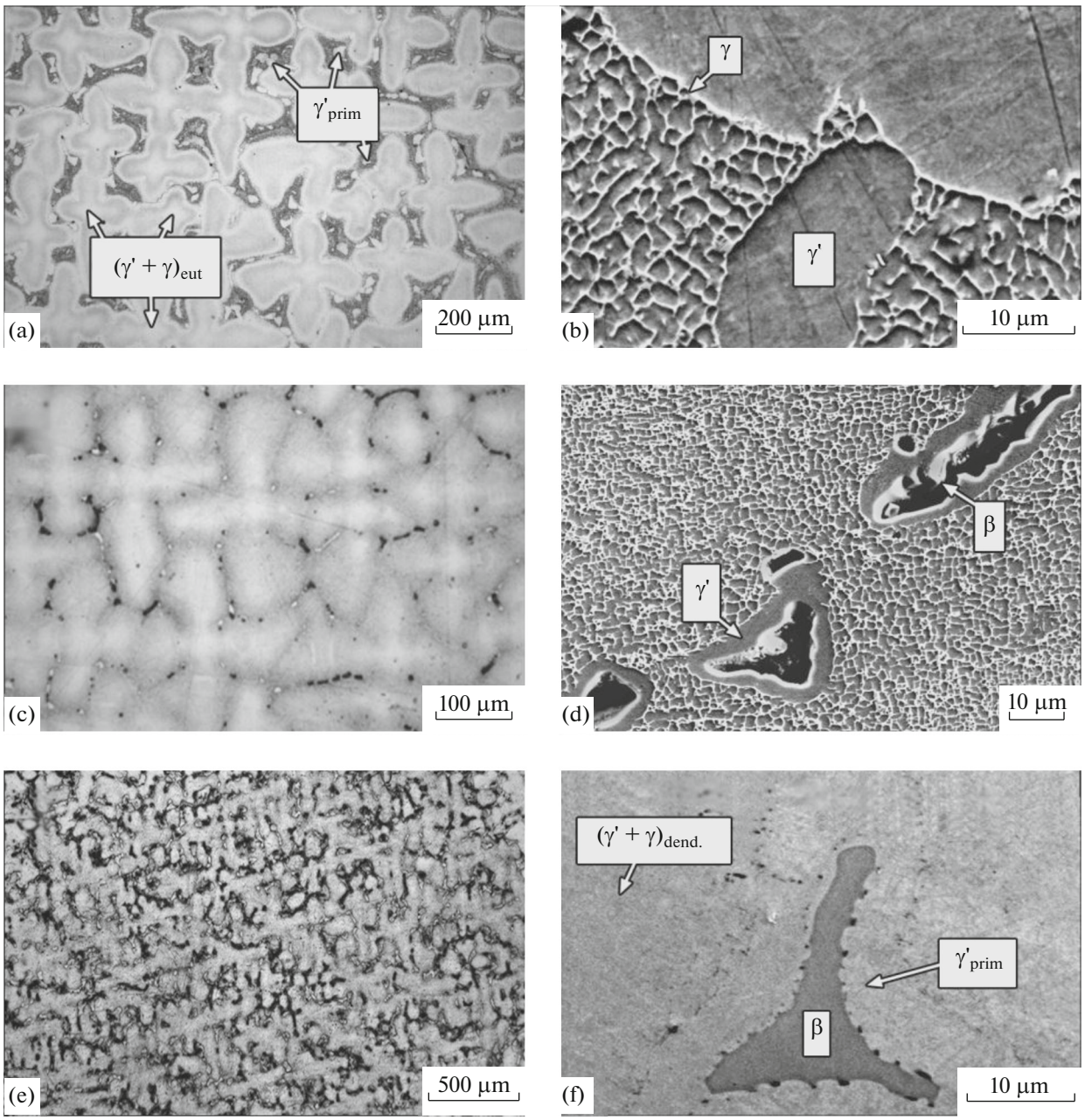

Fig. 2. Microstructures of the cast alloys: (a, b) 17 at % Al, 6 at % Cr, Co-free (VKNA-1V single crystal, $G = 150$°C/cm, $R =$ 10 mm/min); (c, d) 17 at % Al, ~6 at % Cr, ~4 at % Co (VKNA-25 single crystal); and (e, f) 21 at % Al, 7 at % Cr, Co-free (IM730 polycrystal, induction melting with a centrifugal pouring at a rotation rate of 300 min^{-1}). (a, c, e) OM, (d, f) SEM, and (f) BSE.

ture of dendrites in the VKNA-25 alloy is principally different. The γ'-phase portions have a faceting corresponding to CGO of the sample, which is particularly clearly seen in the sample with CGO [111] (Fig. 3c). The structure of dendrites in the IM730 alloy (without Co and Re, but with increased contents of Al and Cr) is the almost pure γ'-phase with a small content of discrete precipitates of the γ-phase, which are nickel-based solid solutions strongly enriched in chromium (20–23 at %).

In the interdendritic space of the VKNA-1V alloy, there are coarse (linear size to 50 μm) single-phase γ'-Ni_3Al inclusions (Fig. 2b) which formed on completing solidification after solidification of dendrites. The solidification of the VKNA-25 is finished via the formation of two-phase precipitates in the interdendritic space: inside the γ'-Ni_3Al phase (composition, at %: 61.45% Ni, 28.5% Al, 1.9% Ti, 3.8% Cr, 3.2% Co, 0.2% W, 0.9% Mo, 0.05% Re), precipitates of the aluminum-enriched phase form (we denoted this

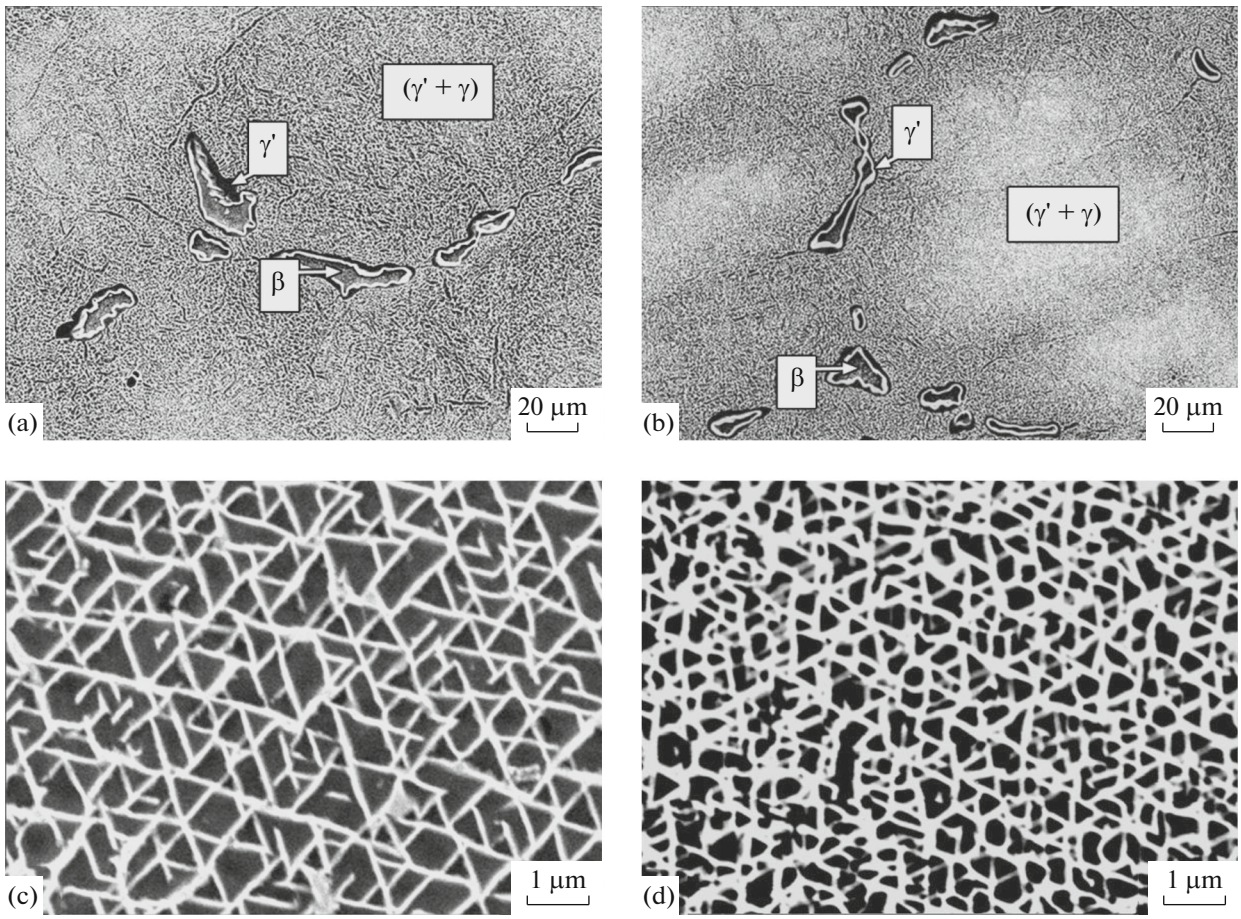

Fig. 3. Microstructures of the [111] VKNA-25 alloy single crystals at a solidification rate R = (a, c) 5 and (b, d) 20 mm/min. (a, b) Inverted SEM image.

phase as β-NiAl in Figs. 2d, 3a, 3b). This phase is revealed on unetched metallographic sections during photography in the BSE mode; it intensively dissolves during etching; as a result, these portions appear as depressions (Fig. 2d). The chemical composition of the phase (in %: 48.35 Ni, 45 Al, 0.3 Ti, 3.6 Cr, 2.4 Co, 0.04 W, 0.3 Mo, 0.01 Re) corresponds to the β-NiAl-based solid solution in the Ni–Co–Al system [19]. The solidification of the IM730 alloy is also finished via the formation of two-phase in the interdendritic space: inside the γ'-Ni_3Al phase, an aluminum-rich phase forms (we denoted this phase as β-NiAl in Fig. 2f). The chemical composition of this phase (in %: 56.6 Ni, 39.4 Al, 3.9 Cr, and 0.1 Mo) corresponds to the β-NiAl-based solid solution in the Ni–Cr–Al system [20]. This phase is observed quite well on unetched metallographic sections during SEM photography in the BSE mode.

The study of the influence of the temperature–time solidification parameters at a constant solidification gradient (G = 150°C/cm) on the structure and the properties of the VKNA-25 alloy showed that the γ' and γ phases in the dendrite axes and (γ' + β) precipitates in the interdendritic regions are refined (Figs. 3c, 3d) as solidification rate R increases from 5 to 20 mm/min; however, the structures of dendrite and interdendritic precipitates are not changed and not dependent on CGO [21].

The single-phase inclusions (Figs. 2b) can be interpreted as degenerate eutectic $L \rightleftarrows (\gamma' + \gamma) + \gamma'$ if the solidification goes by the first variant (Fig. 1a) and the two-phase inclusions (Figs. 2d, 2f, 3a, and 3c) as the degenerate eutectic $L \rightleftarrows (\gamma' + \beta) + \beta$ if the solidification goes by the second variant (Fig. 1b).

The isothermal sections of ternary Ni–Al–Co (Fig. 4a) [19], Ni–Al–Cr (Fig. 4b) [20], Ni–Al–Mo (Fig. 4c) [22], and Ni–Al–W (Fig. 4d) [23, 24] give an indication on the phase composition of cast Ni-Al alloys at subsolidus temperatures as to ~3–7 at % of each of AEs are incorporated to them.

The interdendritic inclusions have a two-phase structure in the VKMA-4U and VKNA-25 alloys with ~17 at % Al and 5–6 at % Cr in the presence of ~4 at % Co, the appearance of β-NiAl in which agrees with the structure of the ternary Ni–Al–Co system (Fig. 4a). The appearance of two-phase precipitates in

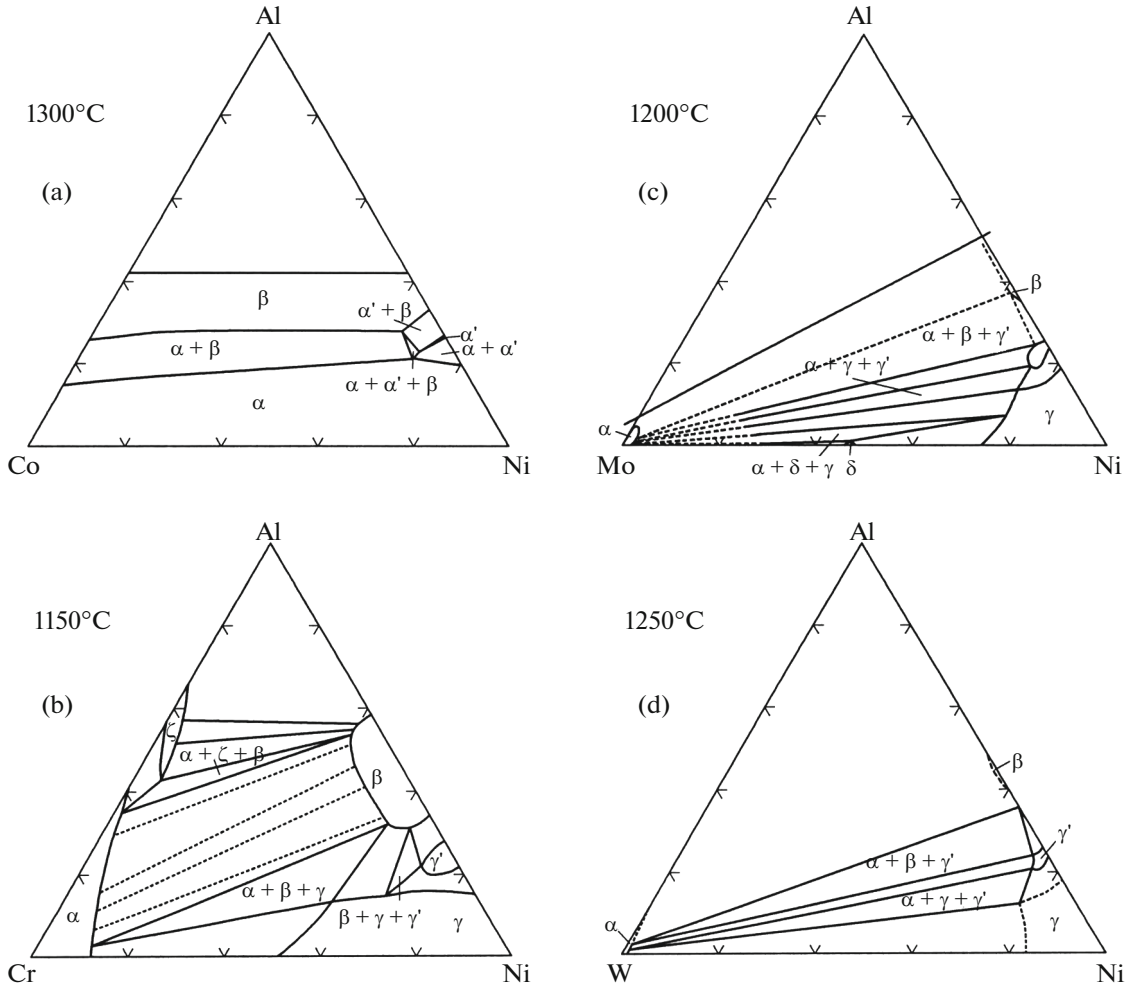

Fig. 4. Isothermal sections of the alloys (a) Ni–Al–Co, (b) Ni–Al–Cr, (c) Ni–Al–Mo, and (d) Ni–Al–W at high (subsolidus) temperatures.

the cobalt-free IM730 alloy with 21 at % Al and 7 at % Cr is more likely to be due to the increase in the aluminum content in the alloy than due to the increase in the chromium content by 1% (Fig. 4b) as compared to the VKNA-type alloys. The content of 2.9–3.8 at % (W + Mo) in the (γ′ + γ) alloys does not influence the appearance of β-NiAl inclusions in the interdendritic γ′-Ni_3Al precipitates as follows from the comparison of the microstructures of the VKNA-1V alloy with 2.8 at % (W + Mo) (there are no β-NiAl inclusions) and IM730 with 1 at % Mo (there are β-NiAl inclusions, Fig. 2f). More likely, a local excess of chromium, molybdenum, or tungsten can lead to the formation of inclusions of nonequilibrium α phases with bcc crystal structures enriched in chromium, molybdenum or tungsten. This assumption correlates with the structures of Ni–Al–Mo and Ni–Al–W phase diagrams (Figs. 4c, 4d).

Obviously, the two-phase (γ′ + β) precipitates are nonequilibrium. The study of the influence of HT on the structure of high-temperature cast (γ′ + γ) alloys showed that, in this case, the phase compositions of the VKNA-4U, VKNA-25, and IM730 alloys are changed (Fig. 5). Even after HT at a temperature of 1200°C for 5 h, the β-phase inclusions inside primary γ′-Ni_3Al precipitates in the interdendritic space disappear (Figs. 5b, 5d); these precipitates are clearly visible in the structures of these alloys in the state after solidification (Figs. 2d, 2f, 3a, 3b, and 5a, 5c). In the VKNA-25 alloy, the boundaries between the (γ′ + γ) dendrites and primary (γ′-Ni_3Al precipitates in the interdendritic space disappear (Fig. 5b).

We focus attention on the significant changes in the morphology and the size and the orientation of the phases in dendrites of these alloys during HT. After solidification of the VKNA-25 alloy, the γ′-phase portions (they have a size one order of value larger than that in the dendrite axes) separated by thin γ-phase interlayers are equiaxial (Fig. 5a). After HT, the γ′-phase portions become extended in the direction transverse to the growth of the secondary dendrite axes (Fig. 5b). The thickness (*d*)-to-length (*l*) ratio is ~1 : 10.

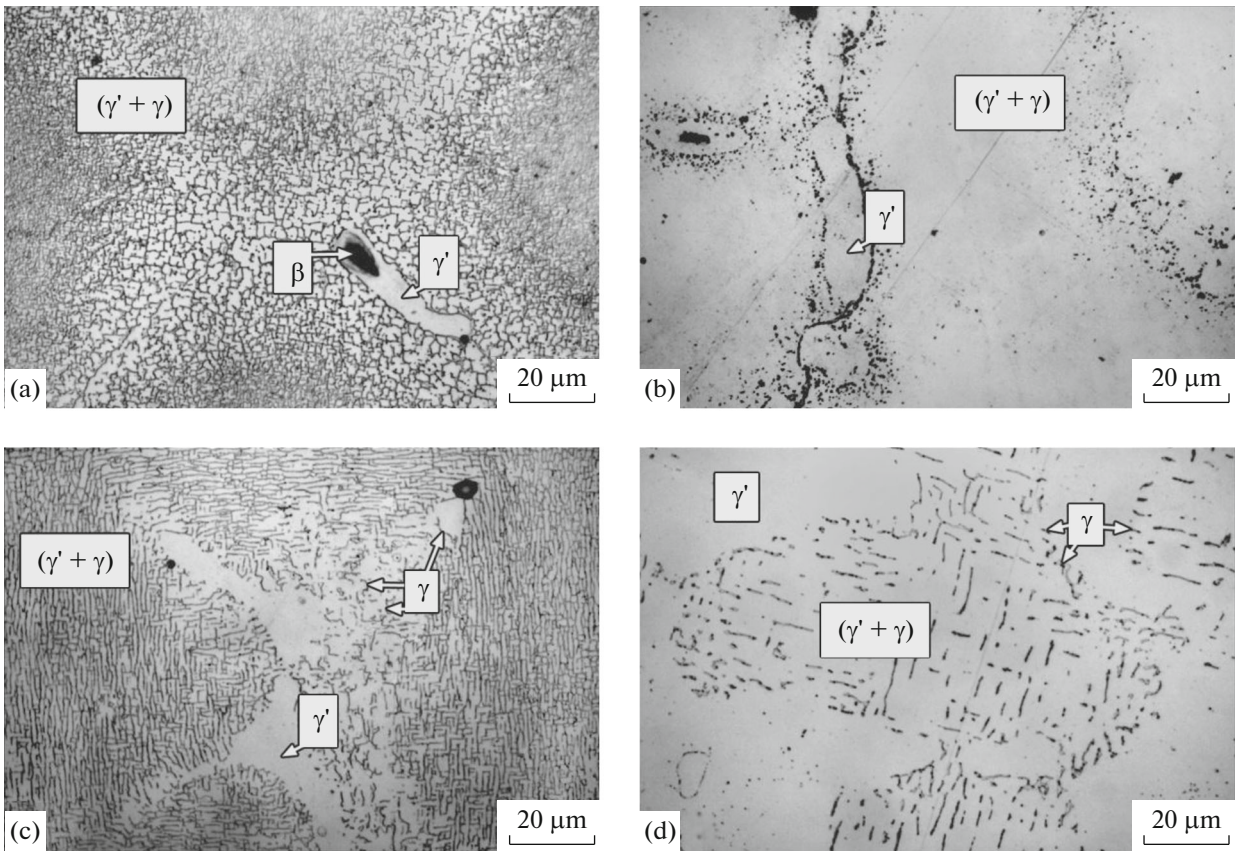

Fig. 5. Microstructures of the (a, b) VKNA-25 and (c, d) IM730 alloys after (a, c) solidification and (b, d) HT at 1200°C for 5 h.

After solidification of the IM730 alloy, the dendrites are almost pure γ′ phase. In the γ′ phase, disperse equiaxial inclusions of the γ phase randomly arranged near the dendrite boundaries are precipitates (Fig. 5c), but they are badly noticeable upon etching. After HT, the rarely arranged γ-phase inclusions take the form of thin (nanosized) extended ($d : l \sim 1 : 20$) plates or rods oriented along the cubic planes in the $L1_2$ crystal lattice of the γ phase of dendrites.

Phase Transformation Temperatures in the (γ′ + γ + β) Alloys on Heating

Figure 6 shows the DSC results obtained for the γ′-Ni_3Al-base alloys after their solidification.

From the DSC curves, it follows that all the curves have peaks related to the alloy melting. Melting starts at the solidus temperatures (T_{solid} = 1325, 1311, 1340, and 1333°C for the VKNA-1V, VKNA-4U, VKNA-25, and IM730 alloys, respectively) and finishes at the liquidus temperatures (T_{liquid} = 1396, 1384, 1408, and 1387°C, respectively). The peak shape (the existence of kinks in the curves between T_{solid} and T_{liquid}) shows that two structural components, namely, initial γ′-Ni_3Al precipitates in the interdendritic space and, at further increase in temperature, (γ′ + γ) dendrites, melt almost simultaneously.

It is noted that there is a principal difference between the DSC curves measured on heating for the cast VKNA-1V alloy (Fig. 6a) and cast VKNA-4U, VKNA-25, and IM730 alloys (Figs. 6b–6d). In the first-type alloys (VKNA-1V and also IC221M, IC218, IC438, IC6SX), there are no β-phase precipitates inside the initial γ′-Ni_3Al precipitates in the interdendritic space (Fig. 2b). The structures of the second-type alloys (VKNA-4U, VKNA-25, and IM730, Figs. 6b–6d), contain the β-phase precipitates (Figs. 2d, 2f, 3a, 3b). In these three alloys, on heating starting from ~800°C, a solid-phase transformation develops, achieves the maximum intensity at temperatures higher than 1200°C (~1266, 1268, 1295°C), and ends at temperatures of ~1291°C, 1283°C, and 1311°C for the VKNA-4U, VKNA-25, and IM730 alloys, respectively.

Because the VKNA-4U, VKNA-25, and IN730 alloys undergo a number of structure–phase transformations during HT at 1200°C for 5 h (dissolution of the β-phase precipitates in primary γ′-Ni_3Al precipitates, which is absent in the first-type alloys, the dissolution or decrease of the interdendritic γ′-phase precipitates, and a change in the morphology and the ori-

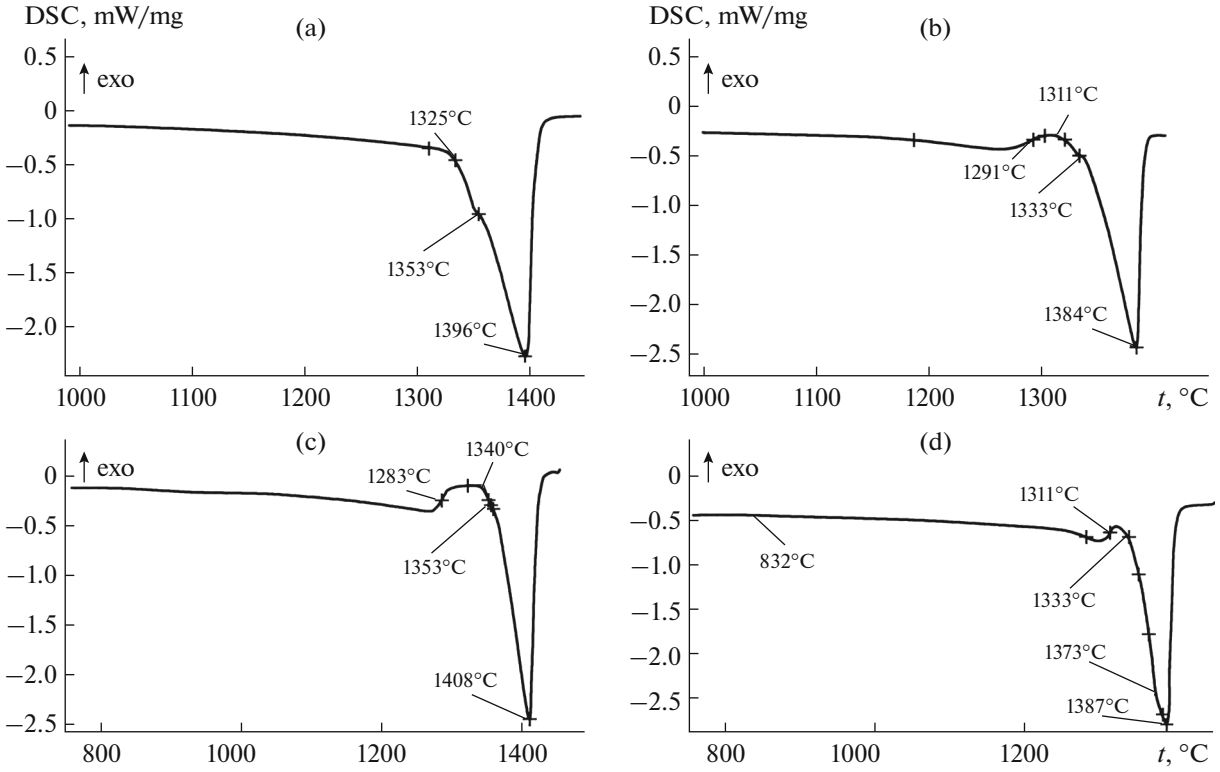

Fig. 6. DSC curves measured on heating for cast (a) VKNA-1V, (b) VKNA-4U, (c) VKNA-25, and (d) IM730 alloys after solidification.

entation of the γ-phase precipitates in dendrites and in the interdendritic space), it can be assumed that the appearance of the peak in the DSC curves at the temperatures preceding the onset of melting is related to these solid-phase transformations.

It should be noted that the existence of the structure-phase transformations at the subsolidus temperatures in the VKNA-4U, VKNA-25, and IM730 alloys demonstrates a lower stability of their structures as compared to that of the VKNA-1V alloy.

CONCLUSIONS

(1) We analyzed the structure of the ternary Ni–Al–AE (AE are the main alloying elements) phase diagrams of high-temperature cast (γ′ + γ) γ′-Ni_3Al alloys Ni–Al–Cr–Mo–Ti(Zr, Hf)-La(B) with W, Re, and Co or without them.

(2) There are principal differences between the solidification schemes in the vicinity of γ′-Ni_3Al and β-NiAl precipitates and between the influences of the main AEs at their contents to 10 at % on the phase compositions of the multicomponent alloys.

(3) The structures of the γ′-Ni_3Al VKNA-1V, VKNA-25, VKNA-4U, and IM730 alloys were studied. The base of all the alloys are (γ′ + γ) dendrites (proportion of the phases is dependent on alloying). In the cobalt-free VKNA-1V alloy, as well as in other first-type alloys, coarse single-phase γ′-Ni_3Al precipitates, which are the degenerate eutectic $L \rightleftarrows (\gamma' + \gamma) + \gamma'$, form in the interdendritic space. In the second-type alloys containing cobalt at the same aluminum content (VKNA-4U and VKNA-25 alloys) or the cobalt-free alloys containing chromium and an increased aluminum content (IM730 alloy), the following two-phase precipitates form: nonequilibrium β-NiAl inclusions, which are the degenerate eutectic $L \rightleftarrows (\gamma' + \beta) + \beta$ form inside the γ′-Ni_3Al phase.

(4) DSC studies showed that the second-type alloys undergo the following structure–phase transformations on heating at subsolidus temperatures (1200–1300°C): the dissolution of the β-phase precipitates in the initial γ′-Ni_3Al precipitates, which is absent in the first-type alloys; the dissolution or a weakening of the interdendritic γ′-phase precipitates; and a change in the morphology and the orientations of the γ-phase precipitates in dendrites and the interdendritic space.

FUNDING

This work was performed according state asignment no. 075-00746-19-00 and was supported by the Russian Foundation for Basic Research, project no. 19-03-00852 a.

REFERENCES

1. E. N. Kablov, B. S. Lomberg, V. P. Buntushkin, E. P. Golubovskii, and S. A. Muboyadzhyan, "Intermetallic Ni_3Al-base alloy: a promising material for turbine blades," Metal Sci. Heat Treat. **44** (7–8), 284–287 (2002).
2. K. B. Povarova, N. K. Kazanskaya, V. P. Buntushkin, V. G. Kostogryz, V. G. Bakharev, V. I. Mironov, O. A. Bazyleva, A. A. Drozdov, and I. O. Bannykh, "Thermal structural stability of an Ni_3Al-based alloy and its application for blades in small gas-turbine engines," Rus. Metall. (Metally), No. 3, 269–274 (2003).
3. K. B. Povarova, A. A. Drozdov, V. P. Buntushkin, N. K. Kazanskaya, and O. A. Bazyleva, "Extra light high-temperature nanostructured Ni_3Al-based alloys for aviation engine building and power engineering," Voprosy Materialoved., No. 2(54), 85–93 (2008).
4. N. A. Nochovnaya, O. A. Bazyleva, D. E. Kablov, and P. V. Panin, *Titanium- and Nickel-Based Intermetallic Alloys*, Ed. by E. N. Kablov (VIAM, Moscow, 2018).
5. H. B. Motejadded, M. Soltanieh, and S. Rastegari, "Coarsing kinetics of γ′ precipitates in dendritic regions of a Ni_3Al base alloy," J. Mater. Sci. Technol. **28** (3), 221–228 (2012).
6. *Phase Diagrams of Binary Metallic Systems. A Handbook in 3 vol.*, Ed by N. P. Lyakishev, (Mashinostroenie, Moscow, 1996 (vol. 1), 1997 (vol. 2), 2001 (vol. 3)).
7. K. Hilpert, D. Kobertz, V. Venugopal, M. Miller, H. Herads, F. J. Bremer, and H. Nickel, "Phase diagram studies on the Al–Ni system," Z. Naturforsch. A **42**, 1327–1332 (1987).
8. *Superalloys II. High-Temperature Materials for Aerospace and Industrial Power* (Wiley, New York, 1987).
9. C. M. F. Rae et al., "Topologically close packed phases in an experimental rhenium-containing single crystal super alloy," in *Super Alloys 2000* (Miner., Metals, & Mater. Soc, 2000), pp. 767–776.
10. C. M. F. Rae and R. C. Reed, "The precipitation of topologically close-packed phases in rhenium-containing super alloys," Acta Mater. **49** (10), 4113–4125 (2001).
11. M. V. Acharya and G. E. Fuch, "The effect of long-term thermal exposures on the microstructure and properties of CMSX-10 single crystal Ni-base super alloys," Mater. Sci. Eng. **381**, 143–153 (2004).
12. O. A. Bazyleva, K. B. Povarova, N. K. Kazanskaya, and A. A. Drozdov, "Cast Ni_3Al-based alloys and the method of their melting," Zagot. Proizv. Mashinostr., No. 1, 29–35 (2010).
13. K. B. Povarova, A. A. Drozdov, M. A. Bulakhtina, A. V. Antonova, A. E. Morozov, O. A. Bazyleva, Y. A. Bondarenko, E. G. Arginbaeva, and D. G. Nefedov, "Effect of the method of producing Ni_3Al-based alloy single crystals on the macro- and microhomogeneity of component distribution, structure, and properties," Rus. Metall. (Metally), No. 5, 382–391 (2014).
14. K. B. Povarova, Yu. A. Bondarenko, A. A. Drozdov, O. A. Bazyleva, A. V. Antonova, A. E. Morozov, and E. G. Arginbaeva, "Effect of directional solidification on the structure and properties of Ni_3Al-based alloy single crystals alloyed with Cr, Mo, W, Ti, Co, Re, and REM," Rus. Metall. (Metally), No. 1, 43–50 (2015).
15. A. A. Drozdov, O. A. Skachkov, P. O. Zhukov, and T. A. Berezina, "Influence of melting on the structure and properties of a Ni_3Al intermetallic alloy," Stal', No. 4, 50–55 (2017).
16. K. B. Povarova, O. A. Bazyleva, A. A. Drozrov, A. E. Morozov, E. G. Arginbaeva, and A. V. Antonova, "Effect of heat treatment on dendrite segregation and high-temperature strength of single crystals of Ni_3Al-base rhenium-alloyed intermetallic alloys," Metalloved. Term. Obrab. Met. **60** (9–10), 594–601 (2019).
17. O. A. Bazyleva, E. G. Arginbaeva, and E. Yu. Turenko, "High-temperature cast intermetallic alloys," Aviat. Mater. Technol., No. 5, 57–60 (2012).
18. O. A. Bazyleva, A. V. Goryunov, T. N. Zagvozdkina, and D. G. Nefedov, "Segregation inhomogeneity of the VKNA-4U MONO alloy and its influence of the properties," Metallurg. Mashinostr., No. 4, 18–21 (2012).
19. M. Hubert-Protopopescu and H. Hubert, "Al–Co–Ni," in *Ternary Alloys: A Comparative Compendium of Evaluated Constitutional Data and Phase Diagrams*, Eds. by G. Petzow and G. Effenberg (VCH Cop., Weinheim, 1991), Vol. 4: Al–Cd–Ce to Al–Cu–Ru, pp. 234–244.
20. P. Rogl, "Al–Cr–Ni," in *Ternary Alloys: A Comparative Compendium of Evaluated Constitutional Data and Phase Diagrams*, Ed. by G. Petzow and G. Effenberg (VCH Cop., Weinheim, 1991), Vol. 4: Al–Cd–Ce to Al–Cu–Ru, pp. 400–415.
21. O. A. Bazyleva, K. B. Povarova, E. G. Arginbaeva, A. V. Shestakov, and A. A. Drozrov, "Influence of the solidification temperature–time parameters on the structure and mechanical properties of nickel aluminide-based alloys," Rus. Metall. (Metally), No. 11, 916–922 (2015).
22. "Al–Mo–Ni" in *Ternary Alloys: A Comparative Compendium of Evaluated Constitutional Data and Phase Diagrams*, Ed. by G. Petzow and G. Effenberg (VCH Cop., Weinheim, 1993), Vol. 7: Al–Mg–Se to Al–Ni–Ta.
23. Z. Alekseeva, "Ni–Al–W," in *Ternary Alloys: A Comparative Compendium of Evaluated Constitutional Data and Phase Diagrams*, Ed. by G. Petzow and G. Effenberg (VCH Cop., Weinheim, 1993), Vol. 8: Al–Ni–Tb to Al—Zn–Zr, pp. 49–57.
24. J. Porovic, "Microstructure and phase equilibria in Ni–Al–W system," Intermetallics **16**, 884–888 (2008).

Translated by Yu. Ryzhkov